**SANDIA REPORT**
SAND2005-6255
Unlimited Release
Printed October 2005

# Directional Neutron Detectors For Use with 14 MeV Neutrons

Nicholas Mascarenhas, Wondwosen Mengesha, Justin D Peel and Duane Sunnarborg

Prepared by Sandia National Laboratories
Albuquerque, New Mexico 87185 and Livermore, California 94550

Sandia is a multiprogram laboratory operated by Sandia Corporation, a Lockheed Martin Company, for the United States Department of Energy's National Nuclear Security Administration under Contract DE-AC04-94AL85000.



Sandia National Laboratories

Issued by Sandia National Laboratories, operated for the United States
Department of Energy by Sandia Corporation.



Available to DOE and DOE contractors from
Office of Scientific and Technical Information
P.O. Box 62
Oak Ridge, TN 37831

Telephone: (865)576-8401
Facsimile: (865)576-5728

Email: reports@adonis.osti.gov
Online ordering: http://www.doe.gov/bridge

Available to the public from
U.S. Department of Commerce
National Technical Information Service
5285 Port Royal Rd
Springfield, VA 22161

Telephone: (800)553-6847
Facsimile: (702)605-6900

E-Mail: orders@ntis.fedworld.gov
Online order: http://www.ntis.gov/help/ordermethods.asp?loc=7-4-0#online

SAND2005-6255
Unlimited Release
Printed October 2005

# Directional Neutron Detectors For Use with 14 MeV Neutrons

## Fiber Scintillation Methods for Directional Neutron Detection

Nicholas Mascarenhas and Justin D. Peel
Instrumentation Systems Engineering

Duane Sunnarborg
Microfluidics

Wondwosen Mengesha
Exploratory Systems Technology

Sandia National Laboratories
P.O. Box 969
Livermore, CA 94551-9956

## Abstract

Current Joint Test Assembly (JTA) neutron monitors rely on knock-on proton type detectors that are susceptible to X-rays and low energy gamma rays. We investigated two novel plastic scintillating fiber directional neutron detector prototypes. One prototype used a fiber selected such that the fiber width was less than 2.1mm which is the range of a proton in plastic. The difference in the distribution of recoil proton energy deposited in the fiber was used to determine the incident neutron direction. The second prototype measured both the recoil proton energy and direction. The neutron direction was determined from the kinematics of single neutron-proton scatters. This report describes the development and performance of these detectors.

**This page intentionally left blank.**

# Contents



# Figures

## Tables

# Preface

This report describes an LDRD project titled "Advanced Neutron Monitors for JTA and Stockpile Monitoring" (LDRD project #52733). The title of this report differs from the title of the LDRD research program because the research may be applicable to a wider audience since the detection techniques can be used beyond the scope of JTA tests.

The report is divided into the following sections:

- **Section 1** is an introduction to neutron detection and outlines the problem.
- **Section 2** describes the first prototype neutron detector. Here the variation of the recoil proton's path length is used to determine the incident neutron flux direction.
- **Section 3** describes the second detector. Here the recoil proton's energy as well as the proton direction is used to determine the incident neutron direction.
- **Section 4** summarizes results from both detectors.
- **References** lists references.

**This page intentionally left blank.**

# Executive Summary

This report describes a three-year research and development program investigating novel directional neutron detectors for Joint-Test Assembly (JTA) and stockpile monitoring. The detectors were prescribed to be small, optimized for 14 MeV neutrons, and immune to X-ray background. Two plastic scintillating fiber detector designs were investigated. The first detector utilizes differences in energy deposited in the fibers due to path length differences of the recoil protons to determine incident neutron direction. The second is a tracking detector. Both the recoil proton energy and direction are used to reconstruct incident neutron direction.

Our studies suggest that the first detector has a poor angular resolution of around 45°degrees. We find that 0.5 mm round fibers achieve the best resolution for this detector.

A promising type of detector is a tracking neutron detector. It uses an 8x8 array of 0.5 mm square fibers. This detector is sensitive to a change in incident neutron direction of better than $10^{o}$. This detector shows good directional performance in the presence of an X-ray to neutron background of $10^{6}$:1. It is the first tracking neutron detector to be developed which can reconstruct the direction of 14 MeV neutrons from kinematics of single neutron-proton scatters.

**This page intentionally left blank.**

# Section 1. Background

## *Introduction*

Many types of neutron detectors have been developed since the discovery of the neutron in 1932 by James Chadwick [1]. These detectors have either counted the number of neutrons and/or measured the neutron energies. Examples are $BF_3$, $^3He$ and plastic or liquid scintillator detectors. Since neutrons have no net charge, neutrons are detected indirectly through either scattering or neutron capture. Neutron capture detectors can be used in groups to determine the direction of the neutron, but scattering detectors can provide directional information from a single detector. Several directional neutron detectors [2-6] have been developed by others prior to this research.

## *Prior Directional Neutron Detectors and JTA Detectors*

Current JTA (Joint Test Assembly) neutron detectors rely on the knock on proton technique. A thin polyethylene sheet is placed in front of a silicon detector. The protons knocked on by the incident neutrons are detected by the silicon detector. However, silicon detectors are very sensitive to any gamma rays or X-rays present.

Another type of directional neutron detector [2] uses four $^3He$ detectors located at the centers of the faces of a block of plastic moderator such that the detectors form a square. The difference in the number of detected neutrons in detectors on opposite sides of the moderator is used to compute the neutron source direction. Such a detector is not compact and moreover has poor directionality above 1 MeV. A third type of detector uses plastic scintillating fibers [3-5]. Prior work with fiber detectors has been reported [4] using high neutron fluences e.g. during Tokamak fusion test reactor (TFTR) operation. SONTRAC [5] is a 3D scintillating fiber imaging spectrometer which is being developed to measure high energy solar neutrons (20-250 MeV). However, SONTRAC is somewhat bulky and is designed to operate at high energies (>20MeV).

## *Scintillating Fiber Directional Neutron Detectors*

We exploited some elements of the neutron-proton scattering in order to deduce the direction of the neutron source. First, the energy of the scattered proton is given by

$$E_p = 4A/(1+A)^2 E_n \cos^2\theta .$$

$E_p$ and $E_n$ are the proton and neutron energies, respectively, and $\theta$ is the angle between the incident neutron direction and the direction of the scattered proton. A is the ratio of the mass of the target nucleus to the neutron mass. Since neutrons and protons have essentially the same mass ($1.67 \times 10^{-27}$ kg), A=1. For neutron-proton scattering this simplifies to

$$E_p = E_n \cos^2\theta$$

If the incident neutrons are mono-energetic; $E_n$ is known and fixed, then $\theta$ is determined from the kinematics of a single proton scatter by detecting the energy and direction of the scattered proton. We used this concept in our tracking detector. Protons are detected as they slow down in the detector and produce scintillation light. The scintillation light is proportional to energy deposited by the proton in the scintillator [7]. Summing the energy from all the fibers hit yields the proton energy.

The second detection method uses the range of the scattered protons in the plastic fibers [4-5]. A 14 MeV proton has a range of ~2.1 mm in plastic. We designed a scintillating fiber detector with fibers that have a width much less than 2.1 mm and a length much greater than 2.1 mm. An aluminum absorber was introduced between fibers to stop protons. The aluminum absorber also reduced the energy deposited by Compton electrons in the detector. When 14 MeV neutrons are incident along the length of the fibers, a large amount of energy is deposited by the high energy protons recoiling along the incident neutron direction. If the detector is positioned with the neutron source normal to the length of the fibers, high energy protons cannot deposit all of their energy in the fibers. The result was a difference in the energy spectrum when the neutron fluence was parallel to the fiber length as opposed to the energy spectrum when the neutron fluence was perpendicular to the fiber length.

## Section 2. The Energy Spectra Detector

We studied the performance of various sizes of Saint Gobain BCF-12 scintillating fibers to determine the fiber shape with the best directional response. Two different fiber shapes were used: square and circular. For each fiber shape, two sizes were used: 0.5 and 1.0 mm. All fibers were 10 cm in length. An aluminum cylinder with a 4x4 lattice of holes was used to house the fibers. All fibers were coupled to a Hamamatsu R980 photomultiplier tube using optical grease. A digital oscilloscope, recorded the data as shown in Figure 1. Data was analyzed offline using Matlab and C++.

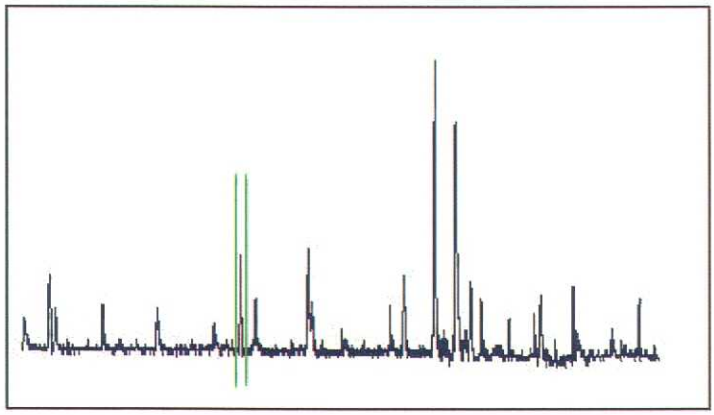

**Figure 1.** Neutron-proton recoil waveforms digitized by a digital oscilloscope.

### *Analysis*

Neutrons recoil in the fibers to produce knock on protons. The protons generate scintillation light as they slow down in the fiber. The light collected is converted to a voltage pulse by a photomultiplier tube (PMT). Each voltage pulse that was above a noise threshold was considered an event. First we identified the signal pulses from the noise in the system as shown in Figure 2. Each pulse peak was either a local maximum or the start of a maximal plateau in the output signal, so our analysis searched for all peaks in the signal ($N_p$). Next, pulse amplitudes were compared to the threshold value. If the peak amplitude was less than the threshold then the peak was set to zero. This process of finding all of the pulses and comparing each to the threshold value was repeated until only those pulses with sufficiently large amplitude remain. This intermediate result, called the reduced data set, consisting of only the pulses that pass the threshold test was further analyzed by using two methods.

The first method was to integrate the charge in each pulse to find the total energy of the event. In this case, double-pulses can cause a problem. It was incorrect to integrate up a double pulse because it represents two distinct events that happened to overlap. Integrating a double pulse as a single pulse would result in a much larger area than any other single pulse in the data. Splitting the double-pulse down the middle at the shared local minima would result in two pulses that have a smaller energy than what the event actually had, so this again was not a viable solution. The easiest solution to the problem that did not produce a bias was to drop the double-pulse from the data set;

however this resulted in dropping useful data. Despite this flaw, dropping double-pulses was the method currently implemented in the integral analysis. Under this method, the number of pulses used ($N_r$) was formalized and written in terms of the total number of pulses in the raw signal ($N_p$), the number of pulses that fail the threshold test ($N_{th}$), and the number of double-pulses ($N_d$) as

$$N_r = N_p - N_{th} - 2N_d$$

The second method used the amplitude of each pulse as an indicator of the total energy of an event. In this case, double-pulses were not nearly as significant because the height of a pulse did not result in a double counting or undercounting of any areas. There was a bias towards a higher magnitude in each pulse of a double-pulse due to the superposition of the two pulses. However, this bias was minimal because each pulse was only 6 to 8 ns wide. The number of pulses analyzed can be formalized as

$$N_r = N_p - N_{th}$$

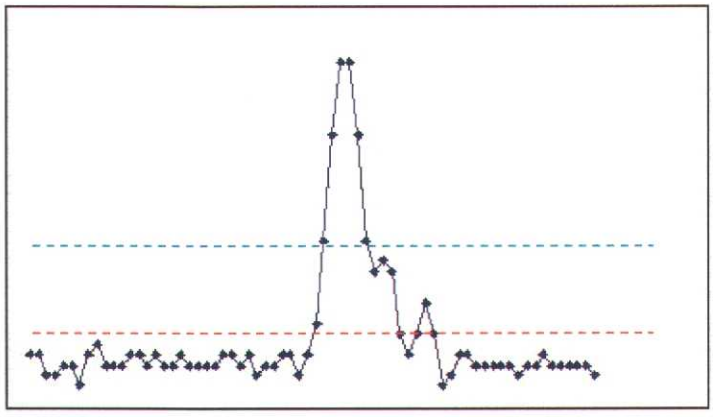

**Figure 2.** A typical recoil proton pulse in a fiber. The dotted lines show two possible thresholds.

The results of each method were then histogrammed (see Figure 3) where the horizontal axis is either the area of an event or the magnitude of an event. This histogram represents the energy distribution profile for the amount of energy deposited by recoil protons in the fibers. We compared the energy distributions for each pair of angles. We examined if there were visible differences between the energy distributions. There were visual differences, so we constructed another step to the analysis to provide a quantitative measurement differences in the two distributions.

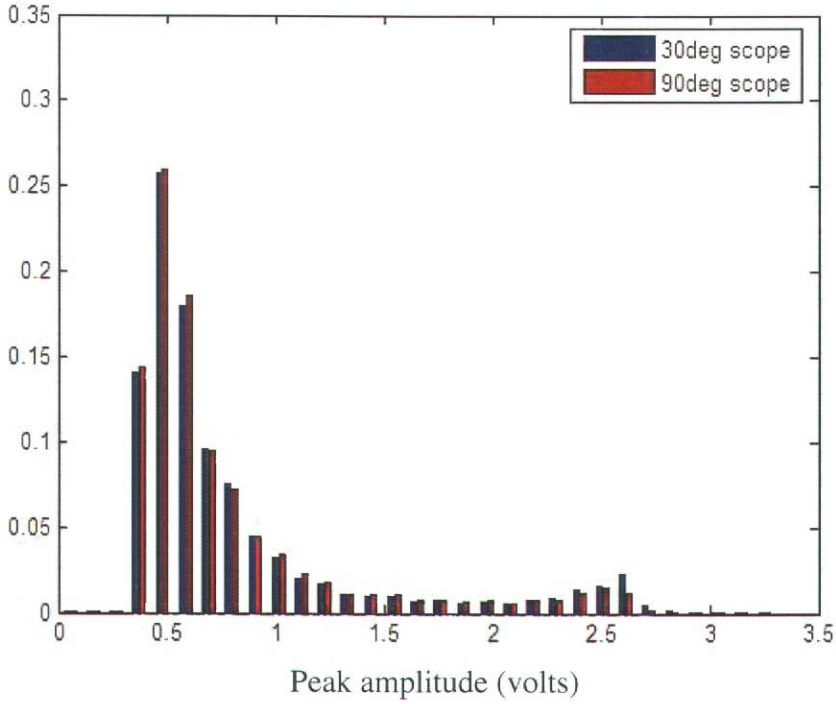


**Figure 3.** A histogram of the recoil proton peaks from neutrons incident at 30° (blue) and 90° (red).

In order to quantitatively show that two histograms are different, we applied a statistical test to examine for differences. Since the expected distribution is not known a priori we made a guess and selected a paired t-test. For the data to fit the requirements for the paired t-test, several assumptions were made. The first assumption was that the counts in each bin are represented as a randomly distributed quantity around a certain mean value for a given total number of counts. The second assumption was that the estimator for the mean of the number of counts in each bin was given by the number of counts recorded in that bin. The third assumption was that the variance of the number of counts in each bin was given by the number of counts recorded in that bin. These three assumptions allowed us to calculate a t-value for comparing the same bin in each pair of angles for each fiber shape. These t-values were used to calculate the quality factor and at what confidence level we could reject the hypothesis that the counts in that bin are the same in favor of the hypothesis that the counts in the higher energy bins was greater for smaller angles. The quality factor measure was simply the average t-value for all bins from a magnitude of 2.0V up to the maximum magnitude of 3.5V excluding all bins in which both distributions have zero counts.

## *Results from the Energy Spectra Detector*

First, we used the integral analysis routines to examine the data from each detector size and shape. Each pair of histograms had little to no visual difference, so the two distributions appeared indistinguishable.

Second, we applied the peak magnitude analysis routines to examine the data from each detector size and shape. In this case, most pairs of histograms appeared visually different, so we tested the histograms using the paired t-test and determined the quality factor (result of the t-test) for each size and shape fiber as shown in Table 1. For 1mm square fibers, the quality factor was 0.201. For 1mm circular fibers, the quality factor was 0.556. This was over twice the quality factor for the 1mm square fibers, so 1mm circular fibers would be a better choice than 1mm square fibers. For 0.5mm square fibers, the quality factor was 1.009. This was significantly larger than the quality factor of either 1mm fiber, so 0.5mm square fiber was preferable to both 1mm fibers. For 0.5mm circular fibers, the quality factor was 1.280. This was better than all of the other fibers, so the distributions for the 0.5mm circular fibers were the most distinguishable.

**Table1.** Results of a t-test study for various fibers. The higher the quality factor the better the directionality. 0.5mm circular fibers show the best directionality

| Fiber Size and Shape | Quality Factor |
|---|---|
| **1mm Square** | **.20100** |
| **1mm Circular** | **.55586** |
| **0.5mm Square** | **1.00932** |
| **0.5mm Circular** | **1.27979** |

## *Summary*

The 0.5mm circular fibers have the highest quality factor which means that on average the pairs of distributions were the most distinguishable. Therefore, the 0.5mm circular fibers would be the best choice for a directional neutron detector using the energy spectra technique.

## Section 3. The Tracking Neutron Detector

The tracking neutron detector (Figure 4) uses Saint Gobain BCF-12 scintillating fibers in an 8x8 square array. The fibers were spaced 2.3 mm apart with an air gap between fibers. The fiber dimensions were 0.5 x 0.5 x 100 mm. One end of each fiber was coupled to an anode of a multi-anode photomultiplier tube (Hamamatsu R5900-00-M64) using optical grease. The fiber assembly was housed in a thin cylindrical aluminum shell which kept the assembly light tight. The fibers were coated with a thin black coating and a black Mylar sheath was placed in between the aluminum shell and the fibers to reduce cross-talk among the fibers. The Bicron fibers were composed of a polystyrene core with an acrylic cladding. The cladding thickness was about 4% of the core size.

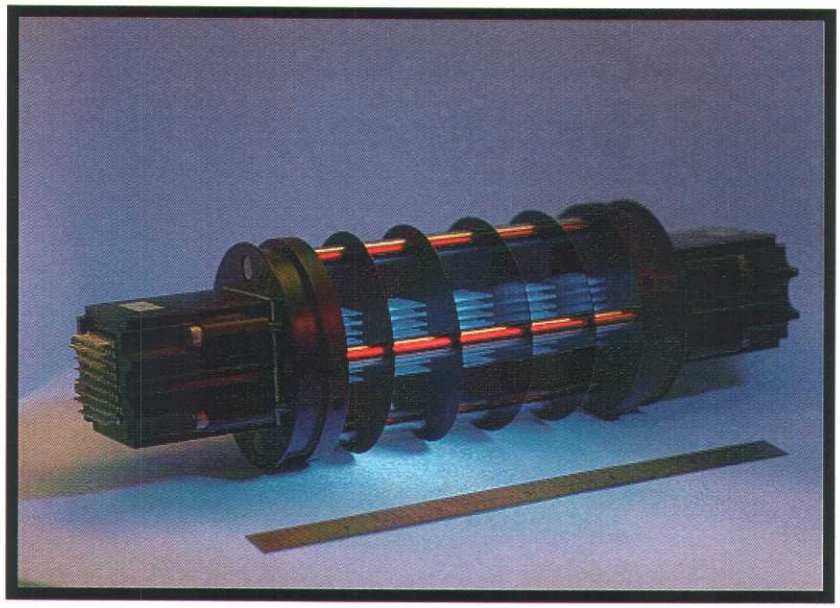

**Figure 4.** The directional neutron detector shown without the aluminum cover. The detector is illuminated by a black light to emphasize the scintillating fibers.

### *Description of the Experimental set-up*

The neutron detector and a VNIIA ING07 neutron generator were placed in a shielded experimental cave, shown in Figure 5. The shielding consisted of 20 cm thick, boron-loaded polyethylene walls to reduce the neutron flux outside the cave. The neutron generator pulsed at 100 Hz with a pulse width of 100 μs. The neutron flux was $8.2 \times 10^6$ neutrons/s. The 14 MeV neutrons are generated isotropically in a D-T reaction. The detector was placed at 0.75m from the source and rotated to various angles to study directionality.

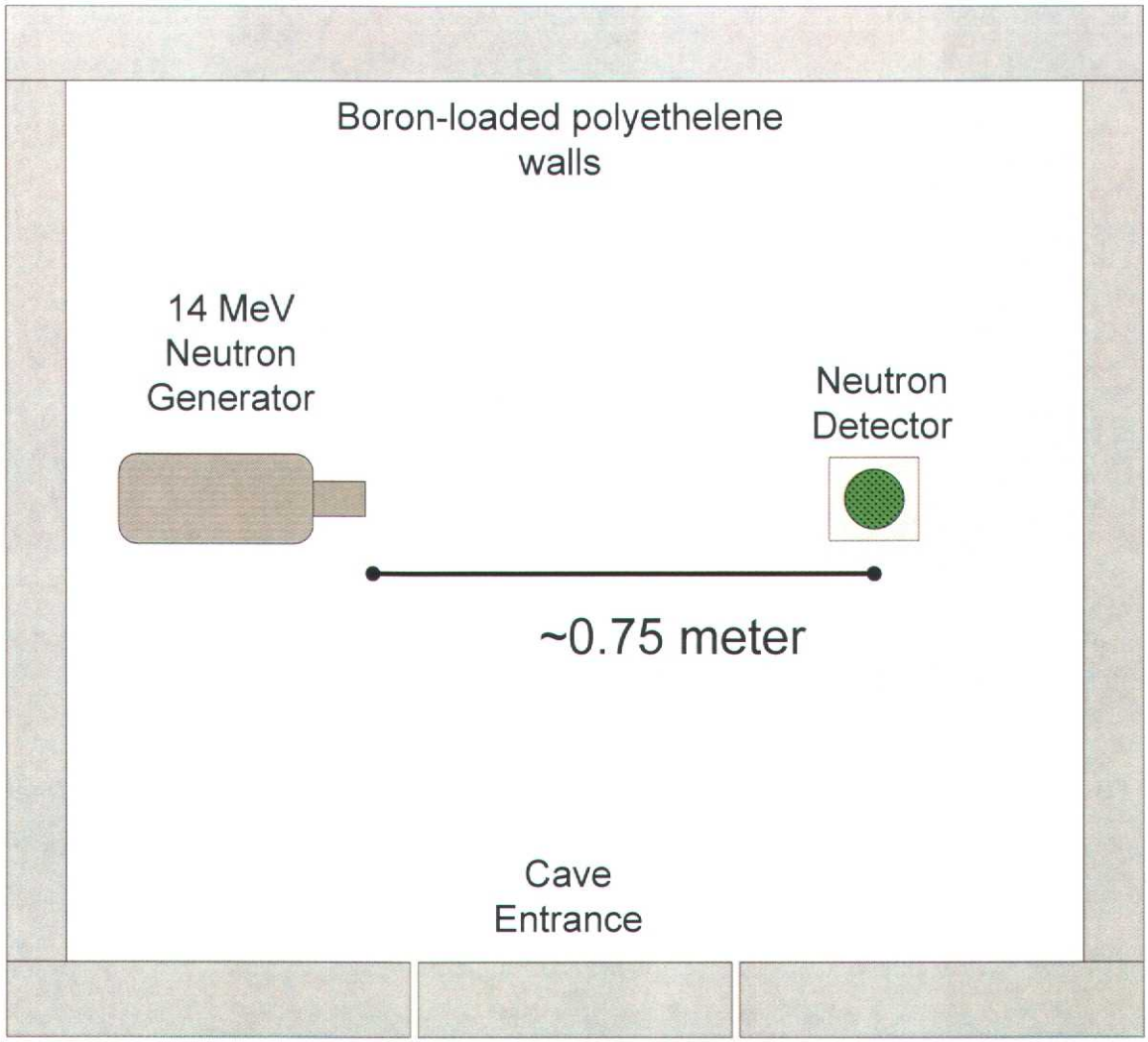


**Figure 5.** The experimental configuration: neutron generator and neutron detector are shown inside the shielded cave.

A flow chart of the data acquisition (DAQ) for this experiment is shown in Figure 6. The DAQ was triggered by a coincidence between the neutron generator and two or more fibers in the detector above a 50 mV threshold. During the duration of the neutron pulse, several neutron-proton recoils could occur in the detector. However, the Analog to Digital Converters (ADC's) have an 8 μs digitization time. During the digitization time we are unable to record multiple neutron events. To reject pile up from multiple neutrons interacting per pulse, we implemented a hardware veto. Subsequent triggers with more than one fiber above a 50 mV threshold during the ADC gate result in both primary and secondary triggers being vetoed.

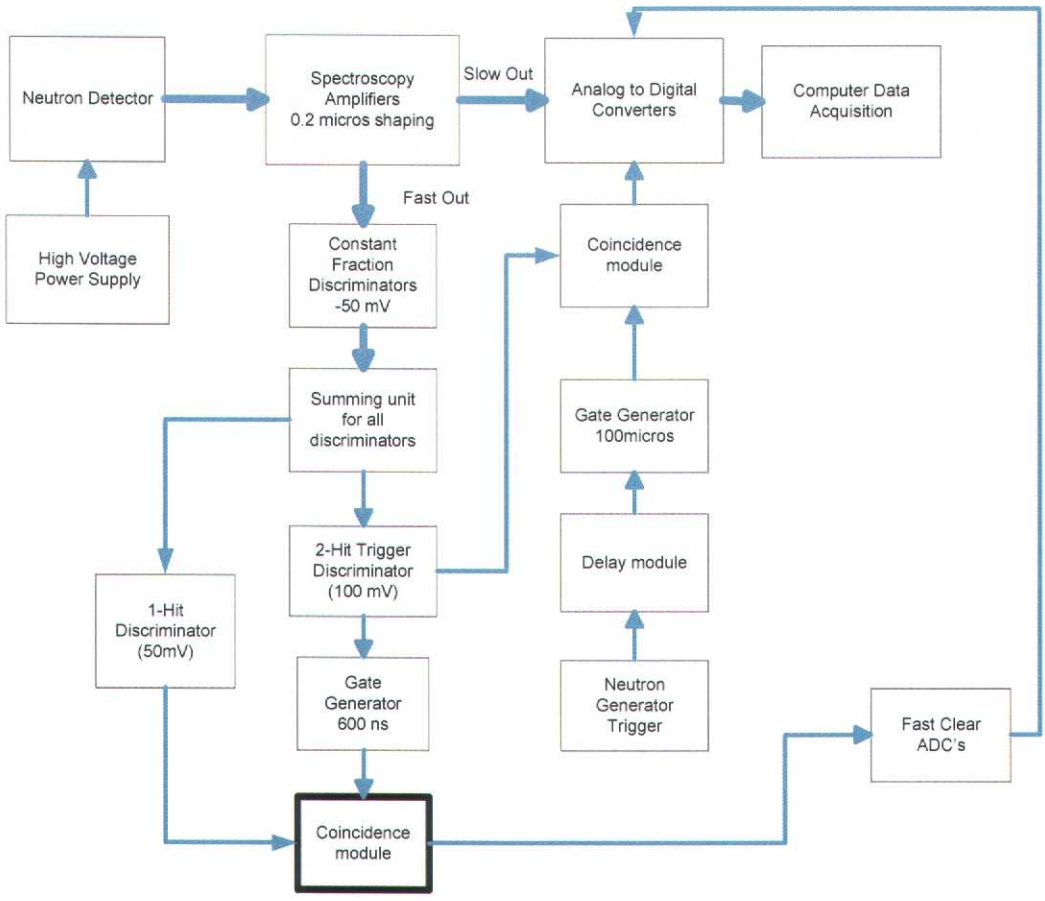


**Figure 6.** A flow chart of the Data Acquisition System (DAQ).

## *Energy Calibration*

We verified particle tracking in the detector (see Figure 7) by using cosmic ray muons. Cosmic ray muons are minimum ionizing and lose about 2.2 MeV/cm in each fiber. For a 0.5mm fiber results in only 0.1 MeV deposited in a fiber with a Landau distribution. This energy is very low compared to the energies of interest (1-14 MeV protons), so cosmic rays were not used for energy calibration but merely to verify track reconstruction and detector functionality. The system linearity was tested by illuminating the fibers with an LED and plotting the mean counts vs. LED amplitude. The plot linearity indicated PMT linearity to different amounts of energy loss.

An energy calibration was performed using 14 MeV neutrons incident along the fiber axis. The resulting proton recoil spectrum in a fiber has an endpoint of 14 MeV. By detecting this end point we determine the detector energy scale. The advantage with using this technique was that the calibration was performed using high energy recoil protons. This was preferred to using cosmic ray muons or gamma ray calibration sources.

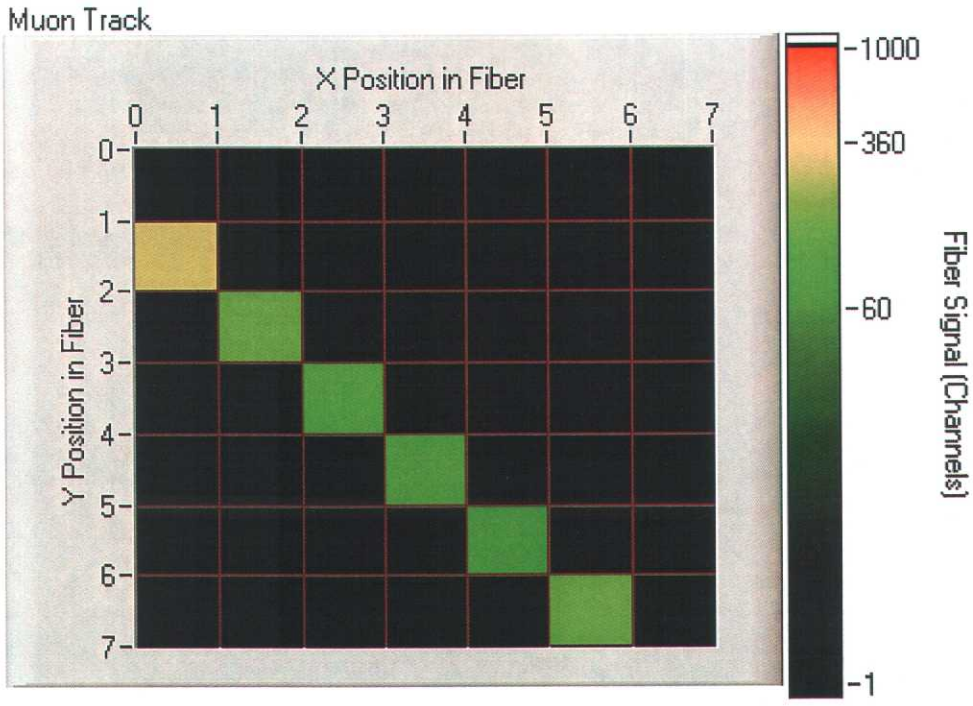


**Figure 7.** A cosmic ray muon track reconstructed with the tracking detector.

## *Reconstructing Neutron Direction*

We reconstruct the neutron direction by using the proton energy and the proton track. In Figure 8 0° is along the positive x-axis. Φ was measured counter-clockwise between the positive x-axis and the proton track. The proton's direction through the detector is arbitrary by 180° because there is no way to distinguish its direction of travel. A Bragg peak could have provided us with this information, but was difficult to resolve in our detector in all cases, so we did not pursue this. Θ was the angle between the proton and neutron paths. From the kinematics of the recoil we derive:

$$\Theta = \pm \cos^{-1}\left(\sqrt{\frac{E_p}{E_n}}\right).$$

The two possible angles arise from the square root in the above equation. Between this sign and the 180° ambiguity in the proton's path, four reconstructed angles will be generated by the equations:

$$\beta = \phi + \Theta$$

$$\beta = \beta + 180°.$$

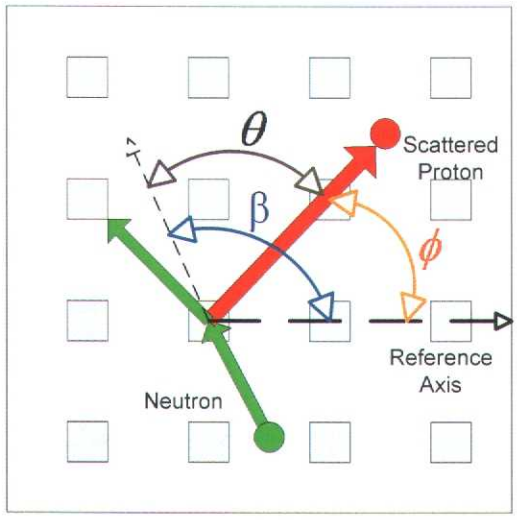


**Figure 8.** Schematic showing the reference frame selected for the fiber detector. The neutron direction β is reconstructed from scattered proton angle Φ and ɵ.

When a large number of events are analyzed, only two peaks will appear with a 180° difference between them. The two additional angles from the ± sign in Θ are uncorrelated and are washed out.

## *Issues Encountered Reconstructing Neutron Direction*

The fiber detector measures a projection of three dimensional proton tracks onto a plane. A result of this 2D readout is the detector can be used for small angles between the incident neutrons and the projection plane. This 2D projection caused a broadening of the peak, but the peak was still quite evident. The reason for this arises in the nature of the interaction. For each event, a neutron scatters off a proton at an angle somewhere in a hemisphere centered on the incident direction of the neutron. For the best case with the neutron direction normal to the length of the fibers, most of the events recorded have a scattered proton that has a very small angle between its travel direction and that of the plane of detection. The result was a broader peak than if the protons were limited to be a two-dimensional scatter. A larger angle between the incident neutrons and the projection plane induces greater broadening in the peak. When neutrons are incident normal to the projection plane, there is no longer any peak.

The tracking neutron detector had several limitations. Proton recoils that overlap within 0.7 μs could not be resolved due to an ADC gate width of 0.7 μs. The CAEN V785 ADC's have a 6 μs conversion time. We were unable to accept a subsequent trigger until after a conversion. This prevented us from reading more than one neutron event per 6 μs. To circumvent this problem, the neutron flux through the detector was lowered until an optimal number of single track events were obtained. In addition we implemented a hardware veto; if a second hit were detected inside a gate both events were vetoed. Residual (unvetoed) multiple tracks events were eliminated from the data by identifying them using a linear fit to the tracks.

Using the simulation tool GEANT4 [8] we developed some improvements to the data analysis. The acrylic cladding around the plastic fibers causes protons to lose about 0.15 MeV each time a proton passed through it. This means that when a proton goes from one fiber to the next, the proton loses a total of 0.3 MeV in the cladding. Energy deposited in the cladding is undetected. The longer the proton tracks the more the undetected energy. There are two ways to handle this.

First, the data analysis can use tracks consisting of two fibers. This minimized the undetected energy loss. In addition, Figure 8 from the simulation showed that requiring one of the fibers to have 5 MeV or more of energy deposited in it generated a better peak because the low energy tracks will have a greater percentage of their energy lost in the acrylic.

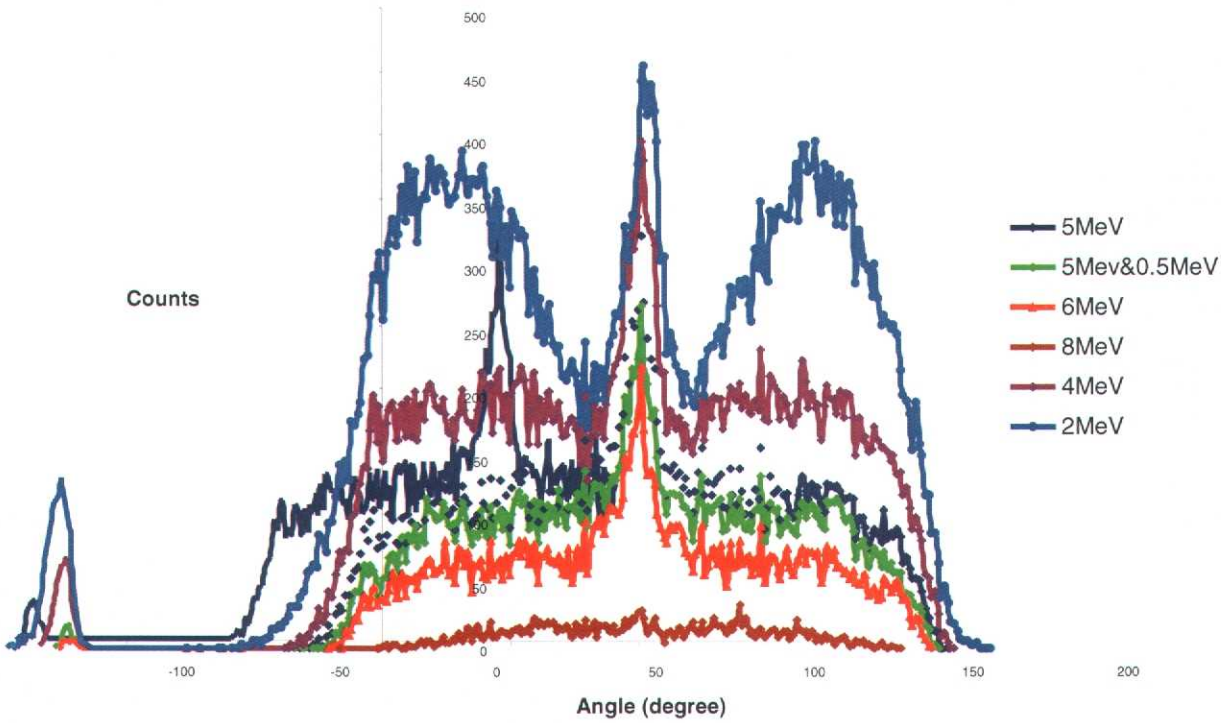


**Figure 9.** Neutron angles reconstructed using various data selection cuts (simulated using GEANT4).

Second, the data analysis could correct for the energy loss in the cladding according to the length of the track. The difficulty in this approach was that the energy loss in the acrylic was dependent on the proton energy.

We also computed the intrinsic detection efficiency for single neutron-proton scatter events using GEANT4 (see Figure 10). Events with 2 fibers hit were a dominant fraction of the data with an intrinsic efficiency of 0.374%. There were few events with ≥ 4 fibers hit.

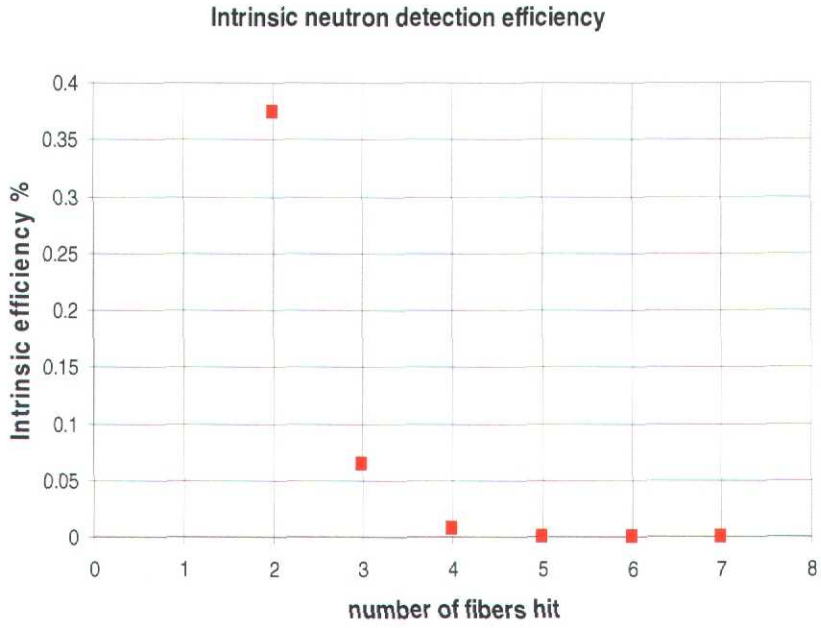


**Figure 10.** The intrinsic neutron detection efficiency computed using GEANT4.

## *Directional Performance*

Figure 11a-d show the detector performance for neutrons incident at 0°, 15°, 23°, and 45°. In each case the two peaks appear separated by 180° due to the ambiguity mentioned earlier. The source direction is given by the mean of the neutron angular distribution. From these studies we find the detector is sensitive to a change in neutron source direction of about 10°.

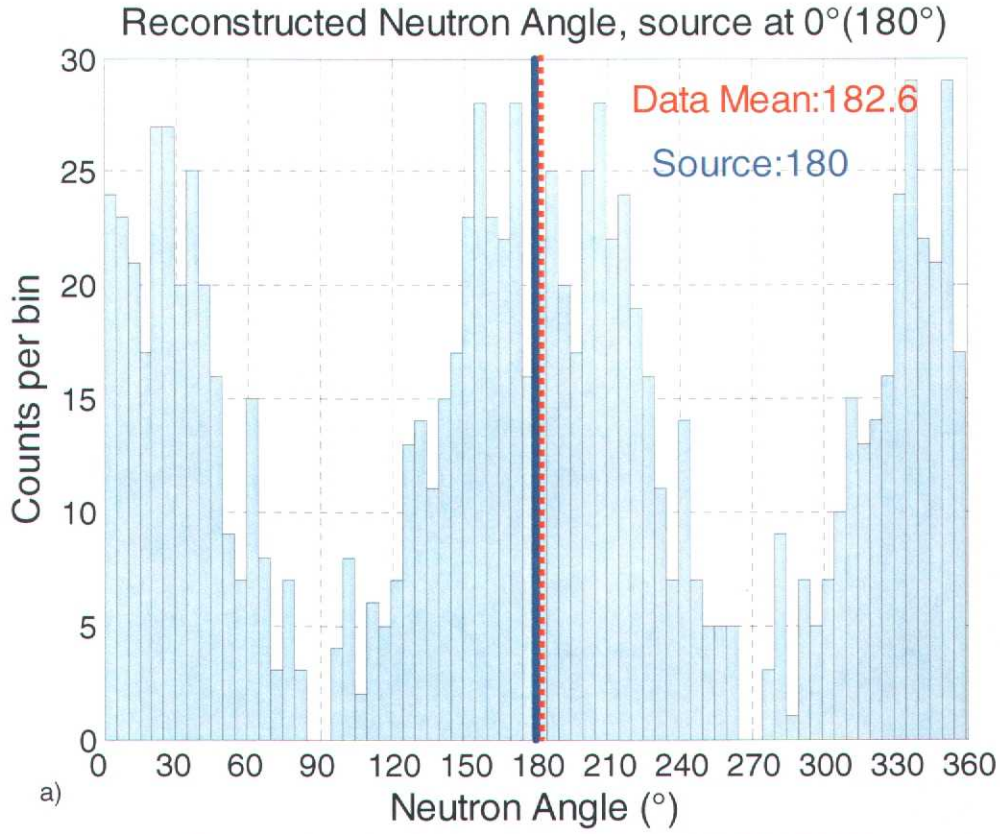
Reconstructed Neutron Angle, source at 0°(180°)
Data Mean:182.6
Source:180
Counts per bin
Neutron Angle (°)
0
5
10
15
20
25
30
0 30 60 90 120 150 180 210 240 270 300 330 360

a)

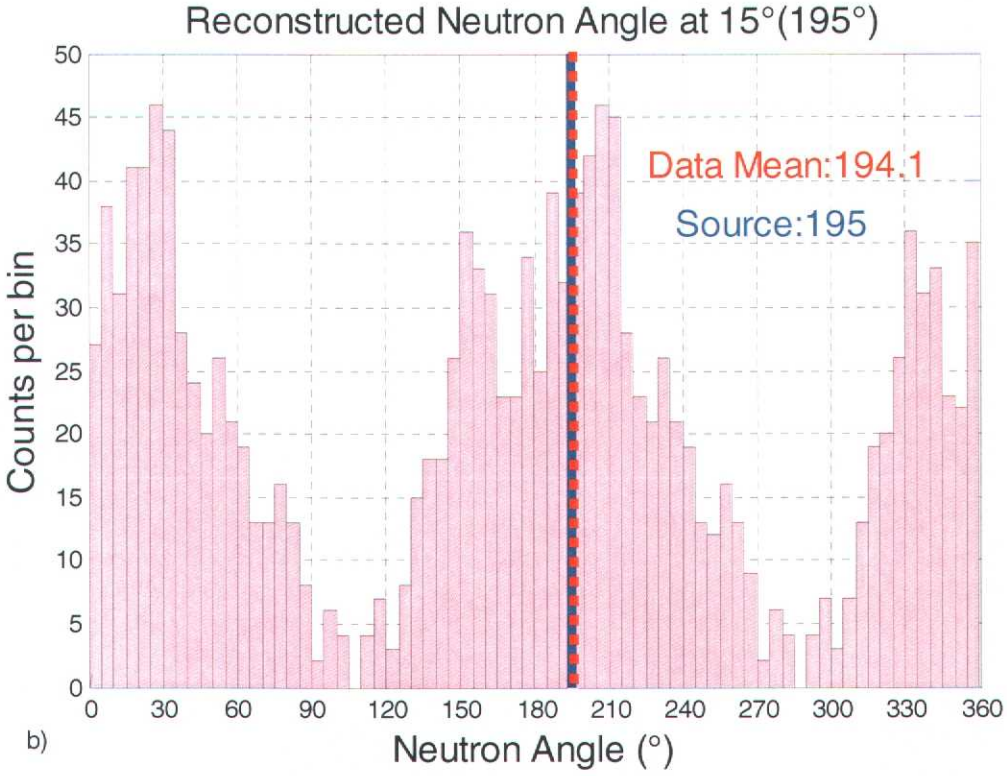
Reconstructed Neutron Angle at 15°(195°)
Data Mean:194.1
Source:195
Counts per bin
Neutron Angle (°)
0
5
10
15
20
25
30
35
40
45
50
0 30 60 90 120 150 180 210 240 270 300 330 360

b)

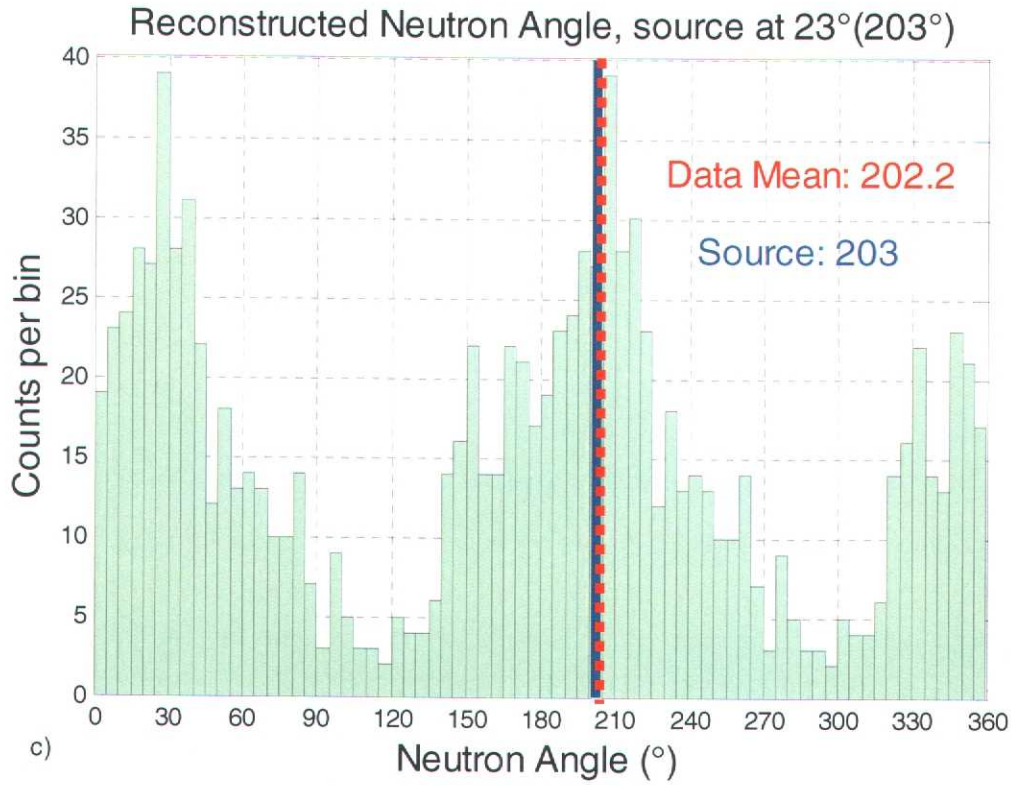


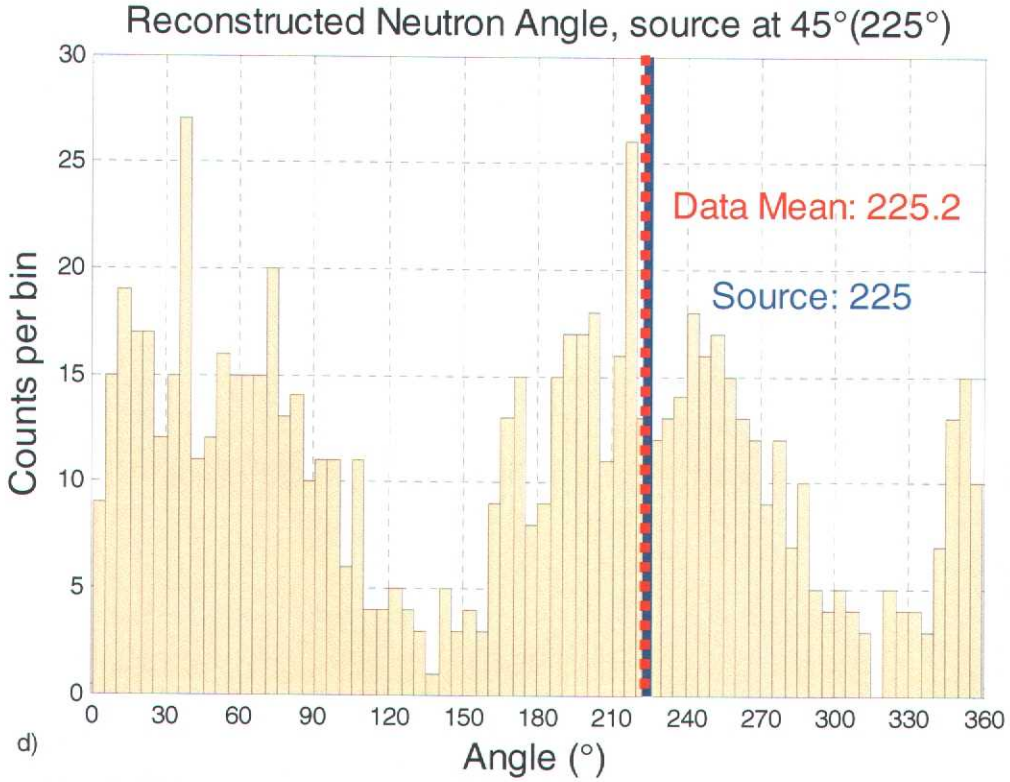


**Figure 11a-d.** Histograms of neutron directions reconstructed using a 14 MeV D-T neutron source. The source direction is varied. The data cuts used are 2 fibers hit with ≥5MeV and ≥0.5MeV in each fiber respectively.

## Detector performance with X-ray background

One of the requirements of the neutron detector for JTA monitoring is to be transparent to X-rays present during the test. In a setting where the detector is isotropically bathed in X-rays, the X-rays create a flat background with the neutron data on top. Silicon detectors used in knock-on proton type neutron detectors are very sensitive to this X-ray background. Scintillating fiber detectors are inherently insensitive to X-rays. This is due to the small fiber cross section (0.5x0.5mm typically) and the multiple Compton scatters that can be identified and rejected. The resulting X-ray signal is a small flat background and can easily be differentiated from the large proton recoil signals.

## Determining the X-ray flux

One of the primary needs of a directional neutron detector for JTA monitoring is the detector immunity to X-rays. A Thermo Kevex X-ray PXS5-925EA source was used to generate X-rays. It is a miniature microfocus X-ray tube that generates bremsstrahlung radiation using a tungsten target. X-rays are generated up to a maximum of 90kV at a max beam current of 0.09mA. The X-ray source produces a 40° cone of X-rays.

A 100:1 ratio of X-rays to neutrons was desired. In order to achieve this, we measured the flux of X-rays from the source. We used a 2" diameter NaI detector to measure this. The high X-rays intensity caused pile up in the detector. To reduce this pile up we placed a 3mm-thick lead collimator with a 1mm diameter hole in front of the detector.

A 1.19mCi Am-241 source (strong 59.539 KeV gamma ray line) was placed at several distances to calibrate detector efficiency. Once the detector efficiency was determined, we varied the X-ray source current and measured the X-rays detected. The number of X-rays scaled linearly with the tube current. From this we were able to calculate the X-ray flux desired at the neutron detector for a given tube current.

## Results of the X-Ray Study

We studied the fiber detector immunity to X-rays using the VNIIA ING07 neutron generator and the Kevex X-ray source simultaneously. For the flux of neutrons used in our measurements the ratio of X-rays to neutrons was set to be about $10^6$:1. For JTA monitoring the ratio needs to be about 100:1. Figure 12 shows the neutrons direction reconstructed with the source neutrons incident at 0°. The tracking neutron detector was found to function well even in this severe X-ray environment. There was no degradation in directional response. The overall raw trigger rate (any two fibers with ≥0.5 MeV deposited in each fiber, no other cuts) increased by only 25%.

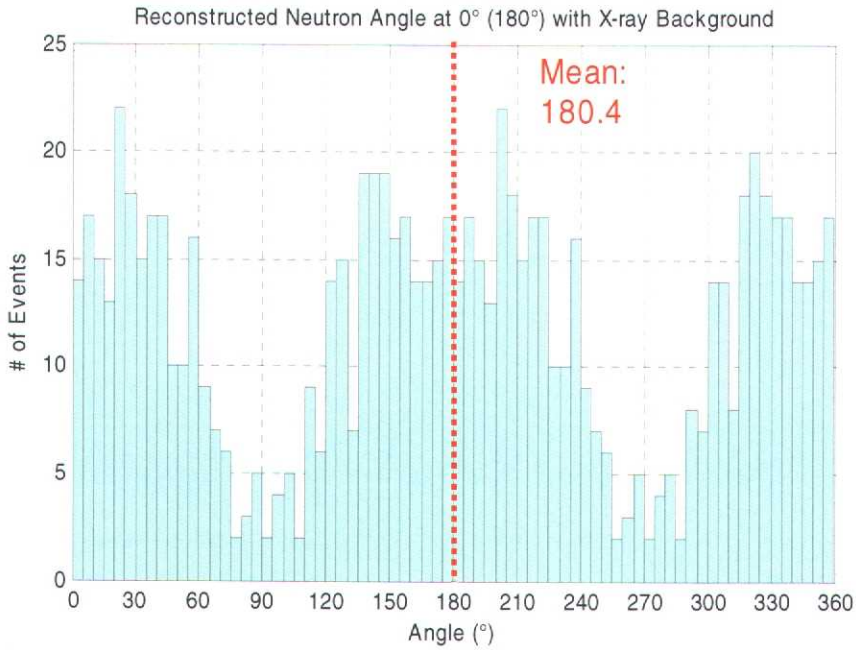


**Figure 12.** Neutron direction reconstructed in the presence of an X-ray background.

**This page intentionally left blank.**

# Section 4. Conclusion

We studied two types of directional neutron detectors using plastic scintillation fibers. The first detector was an energy spectra detector which had a poorer angular resolution (about 45 degrees). It showed optimal performance with 0.5mm round fibers. The second was a novel tracking neutron detector that used 64 0.5mm x 0.5mm x 100mm square fibers. It is sensitive to changes in neutron source direction of about 10 degrees. The detector is compact and shown good directional response with 14 MeV neutrons. We studied the directional performance in the presence of X-rays. A Kevex X-ray generator simulated X-ray background present during JTA tests. X-rays with a 90 kV end point spectrum were used. The tracking detector shows good directional performance in an X-ray to neutron background of $10^6$:1. We developed a detailed model of the tracking neutron detector using GEANT4. The simulations suggested the use of 2 fibers hit with ≥ 5 MeV in one fiber and ≥0.5 MeV in the other to reconstruct the neutron direction with the best resolution. The intrinsic neutron detection efficiency for these 2 fiber events was computed to be 0.374%. Due to limitations in readout electronics we could only capture one neutron scatter event per pulse from the neutron generator. This readout limitation could be overcome in the future using a flash ADC and ring buffer. It may then be possible to accommodate a high neutron rate environment.

## *Acknowledgments*

We thank several people for their assistance with this project. Jason Zaha helped with control software and Labview code. W. Ross Dunkel and Travis McQueen contributed to experiments during their student internships at Sandia/CA. Jim Brennan assisted us with detector fabrication. Jim Lund provided support and guidance throughout this project.

## *References*

[1] J. Chadwick, *Proc. Roy. Soc.* 136 (1932) 692.
[2] H. Yamanashi, *Nucl. Instr. And Meth.* A. 544 (2005) 643.
[3] S. Singkarat, et al., *Nucl. Instr. and Meth.* A 384 (1997) 463.
[4] G.A Wurden, et al., *Rev. Sci. Instrum.* 66 (1), (1995) 901.
[5] R.S. Miller, et al., *Nucl. Instr. and Meth.* A. 505 (2003) 36.
[6] D. Holslin, D. Shreve, and B. Hagan, *Proc. of SPIE Neutrons, X Rays, and Gamma Rays*, 1737 (1992) 14.
[7] R.L. Craun and D.L. Smith, *Nucl. Instr. and Meth.* 80 (1970) 239.
[8] S. Agostinelli et al., *Nucl. Instr. and Meth.* A. 506 (2003) 250.

**This page intentionally left blank.**

## Distribution list

| | | |
|---|---|---|
| 5 | MS9956 | N. Mascarenhas, 8232 |
| 1 | MS9101 | J. Lund, 8232 |
| | | |
| 2 | MS9018 | Central Technical Files, 8945-1 |
| 2 | MS0899 | Technical Library, 4536 |
| 1 | MS 0188 | D. Chavez, LDRD Office, 1011 |

**This page intentionally left blank.**